



HAL
open science

Experimental observation on a laterally loaded pile in unsaturated silty soil

Leonardo Lalicata, Augusto Desideri, Francesca Casini, Luc Thorel

► **To cite this version:**

Leonardo Lalicata, Augusto Desideri, Francesca Casini, Luc Thorel. Experimental observation on a laterally loaded pile in unsaturated silty soil. *Canadian Geotechnical Journal*, 2018, 35p. 10.1139/cgj-2018-0322 . hal-01945314

HAL Id: hal-01945314

<https://hal.science/hal-01945314>

Submitted on 5 Dec 2018

HAL is a multi-disciplinary open access archive for the deposit and dissemination of scientific research documents, whether they are published or not. The documents may come from teaching and research institutions in France or abroad, or from public or private research centers.

L'archive ouverte pluridisciplinaire **HAL**, est destinée au dépôt et à la diffusion de documents scientifiques de niveau recherche, publiés ou non, émanant des établissements d'enseignement et de recherche français ou étrangers, des laboratoires publics ou privés.

1 **Experimental observation on a laterally loaded pile in**
2 **unsaturated silty soil**

3 L.M. Lalicata & A. Desideri

4 *Dipartimento di Ingegneria strutturale e geotecnica. Sapienza Università di Roma. Rome, Italy.*

5 F. Casini

6 *Dipartimento di Ingegneria Civile e Ingegneria Informatica, Università degli Studi di Roma "Tor Vergata",*
7 *Rome, Italy.*

8 L. Thorel

9 *IFSTTAR, GERS Department, Geomaterials and Modelling in Geotechnics Laboratory, Bouguenais, France.*

10

11

Abstract: An experimental study has been carried out to investigate the effects of soil partial saturation on the behaviour of laterally loaded piles. The proposed study has been conducted by means of centrifuge tests at $100\times g$, where a single vertical pile has been subjected to a combination of static horizontal load and bending moment. The study has been conducted on a silty soil characterized with laboratory testing under saturated and unsaturated conditions. During flight, two different positions of water table have been explored. The influence of density has been investigated compacting the sample with two different void ratio. Finally, the effects of a variation of saturation degree on the pile response under loading have been studied rising the water table to ground surface. Data interpretation allows drawing different considerations on the effects of partial saturation on the behaviour of laterally loaded piles. As expected, compared to saturated soils, partial saturation leads always to a stiffer and resistant response of the system. However, the depth of the maximum bending moment is related to the position of water table and the bounding effects induced by partial saturation appears to be more important for loose soils.

Key words: Centrifuge modelling; unsaturated soils; soil-structure interaction; piles; lateral loading

12

13 Introduction

14 The significant soil volume interested by the kinematics of piles foundation under lateral loading
15 is typically limited vertically in the first meters (several diameters of pile) of depth from ground level.
16 A number of studies available in literature (Banerjee and Davies, 1978; Randolph, 1981; Krishnan et
17 al.,1983 Higgins et al., 2013, Di Laora and Rovithis, 2015) point out that, in this class of problems,
18 the system response is mainly influenced by relative pile soil stiffness ratio, opportunely evaluated in
19 the significant volume of soil, while for short and rigid piles response is affected both by stiffness
20 and slenderness ratio. Most relevant parameters such as head displacement and rotation, maximum
21 bending moment and its position along pile length are also strongly influenced by non-linear stress-
22 strain relationships of soils (Budhu & Davies 1987, 1987; Russo, 2016).

23 The behaviour of pile under lateral loading depending, among others factors, from the stiffness
24 of the pile and of the soil surroundings. It is well known that a flexible (or long) pile is characterized
25 by no variation of load or displacement at the tip level during lateral loading at the head. While, a
26 perfectly rigid (or short) pile should behaves with a constant rotation all along its length. The reality
27 is often in between those idealised two extremes cases.

28 In many applications, the significant volume of soil can be above the water table, hence in partial
29 saturation conditions. Nowadays, the effects of suction and saturation degree on the mechanical
30 behaviour of soils have been widely investigated by laboratory studies (Fredlund et al 1978; Cui &
31 Delage 1996; Escario & Saez, 1986; Vassallo et al., 2007; Casini, 2008; Casini et al., 2012; Biglari *et al.*,
32 2011; Sivakumar and Wheeler 2000; Salager et al 2013, Hamid & Miller 2009). In the last years, some
33 studies have been published on the influence of partial saturation in engineering problems such us
34 bearing capacity of shallow and deep foundations (Georgiadis *et al* 2003; Vanapalli 2009). However,
35 in soil-structure interaction problem, potential benefits of suction are often neglected by practical
36 applications.

37 Physical centrifuge modelling represents a valid methodology to experimentally investigate soil-
38 structure interaction problems. The small scale model is linked to the full scale prototype, following
39 scaling laws (e.g. Corté, 1989; Schofield ,1990). When the scale of the model is $1/N$, the model has

40 to be subjected to a centrifuge g -level of N . Studies were so far conducted on fully saturated or
41 completely dried soil model. Only recently, due to a better understanding of the behaviour of
42 compacted soils (Thorel *et al.*, 2011; Caicedo *et al.*, 2014) for the preparation of soil model and to the
43 new instrumentation available to measure suction and saturation degree during the tests (Caicedo and
44 Thorel, 2014; Soranzo *et al.*, 2015), unsaturated soil behaviour has been explored by centrifuge
45 modelling (Casini 2008, Thorel *et al.*, 2011, Soranzo *et al.*, 2015). Scaling laws for unsaturated soils
46 have been experimentally investigated by Depountis *et al.* (2001) and Caicedo *et al.* (2006). The authors
47 found that capillary rise and diffusion time in the centrifuge could be scaled of $1/N$ and $1/N^2$
48 respectively. Details of analytical formulation can be found in Caicedo and Thorel (2014) and Soranzo
49 *et al.* (2015). The scaling factors adopted in this study are listed in Table 1

50 The current experimental study is focused on the influence of partial saturation on the behaviour
51 of laterally loaded pile. The aim of the experiment is to study the response of a single vertical free-
52 head pile, embedded in a homogenous fine graded soil, subjected to a combination of lateral loading
53 and bending moment, under different hydraulic condition and initial void ratio. The study has been
54 developed by means of physical modelling in macro-gravity ($N=100\times g$) using the IFSTTAR
55 centrifuge facilities of Nantes (Rosquoët *et al* 2007).

56 The study is organized as follows. First, model and instrumentation set up are reported. Secondly,
57 the soil hydro-mechanical characterization is briefly presented together with the results of flooding
58 test in oedometer apparatus conducted to explore volumetric behaviour during wetting. Thirdly, soil
59 model preparation and test procedures are presented and described. Finally, the results of the study
60 are discussed focusing the attention on the load-head displacement relationship and flexural pile
61 response, exploring the influence of the different structure and soil saturation conditions. In the last
62 section, the effects of a variation of saturation degree on the pile behaviour are analysed.

63 **Experimental facilities**

64 SOIL PROPERTIES

65 The material used is a commercial kaolin named B-Grade kaolin. The soil has a fine silt fraction
66 of about 90% and a clay fraction of 10%. As reported in Table 2, the material has a liquid limit (w_L)

67 of 42%, a plastic limit (w_p) of 28% and therefore a plastic index (IP) of 14%. The main hydro-
68 mechanical saturated parameters are summarized in Table 2.

69 In order to define the after compaction conditions (w , e) for centrifuge models, a number of
70 flooding experiments have been performed on samples with different compaction features with a
71 constant vertical stress $\sigma_v=150$ kPa. This load corresponds approximately to the vertical stress
72 exerted at half of pile embedded length ($z \cong 8$ m).

73 Tests are carried out in oedometric apparatus of 70 mm in diameter and 18 mm thick. Following
74 the standard procedure proposed by several authors (Wheeler & Sivakumar, 1995; Tarantino & De
75 Col; 2008), the soil has been preliminarily dried at 105 °C for 24 hours then demineralized water has
76 been added to reach the desired water content. The material has been kept in sealed bags for 24-48
77 hours. The specimens have been statically compacted ($v=1.5$ mm/min) directly in the oedometric
78 ring, allowing to reach quite accurately the required void ratio.

79 The tests consist of two steps:

- 80 • Load at constant water content;
- 81 • Soaking at constant load;

82 The grid of water content and void ratio has been chosen on the base of the results of the Standard
83 Proctor test, black line in Figure 1, from which results an optimum water content (w_{opt}) of 0.21 and
84 an optimum void ratio (e_{opt}) of 0.74 (optimum dry density $\gamma_{d,opt}=1.528$ gr/cm³). Three voids ratio are
85 taken into account ($e_0 = 0.77, 0.92$ and 1.12), for water content ranging from 10% to 26%, with steps
86 of 4 %, in order to cover both *dry* than *wet side* of the Proctor curve, Figure 1. For each grid point at
87 least two samples are tested.

88 Moreover, samples conditions after soaking, are presented in Figure 1 with grey symbols, grouped
89 for initial void ratio. All the samples have elevated values of saturation degree, from 0.95 to 1.0. A
90 significant influence of initial void ratio can be recognized: more compacted ($e_0=0.77$) soil shows a
91 little swelling during wetting while the others exhibit collapse deformation during soaking increasing

92 with initial void ratio. A negligible influence of compaction water content on the deformation upon
93 wetting has been found for this material.

94 Based on the experimental results obtained, reported in Figure 1, in order to have a collapsible
95 and a swelling soil sample upon wetting, two initial void ratio are selected (0.93 and 0.75) respectively
96 with the same water content w (0.15).

97 The soil water retention curve (WRC), obtained using the suction controlled oedometric cell
98 (Romero et al. 1995), is presented in Figure 2 in terms of suction and saturation degree relationship.
99 Experimental data refer to the main wetting curve obtained for two different void ratios, 0.93 and
100 0.75 respectively; both of them has been fitted using Van Genuchten (1980) equation the parameters
101 of which are reported in Table 3. In the suction range experimentally studied, as porosity decrease air
102 entry value ($1/\alpha$) increases from 50 to 166 kPa and the slope of the transition (n) zone reduces from
103 1.4 to 1.3 in the S_r-s plane. The findings are consistent with literature results (Gens *et al.*, 1996;
104 Romero, 1999; Romero & Vaunat, 2000; Fredlund & Xing, 1994; Tarantino & De Col, 2008, Romero
105 *et al.* 2011). Neglecting for the sake of simplicity the hysteresis of WRC, the as-compacted suction,
106 according to Van Genuchten (1980) equation, is respectively 900 kPa and 3400 kPa for $e_0=0.93$
107 ($S_{r0}=0.43$), and $e_0=0.75$ ($S_{r0}=0.52$).

108 MODEL AND INSTRUMENTATION

109 For the purpose of the experiment, 180 mm of soil are statically compacted imposing a constant
110 displacement rate ($v=1.5$ mm/min), under one-dimensional condition, in a rigid cylindrical container
111 of 300 mm of diameter. A 10 mm thick sand layer, surrounded by geotextile, is laid as drainage layer
112 at the bottom of the model. A 2 mm thick plastic sheet is placed at the border to reduce the
113 container's roughness and shear stresses developing during model preparation. To prevent water
114 evaporation in the upper part of the model, a plastic film covers the soil surface. The bored pile is
115 installed at $1\times g$, the pre-hole has been realized by means of a manual screwing system of the
116 IFSTTAR facilities (Khemakhem et al., 2010) for an embedded length of 150 mm.

117 The bottom of the model is connected to a water reservoir the level of which is governed by an
118 electro-pneumatic valves system directly controlled by the operator in the centrifuge control room.
119 A laser sensor measures the water height in the tank.

120 The model has been extensively instrumented in order to follow both the equalization phases and
121 pile loading, a schematic view of the instrumentation used is proposed in Figure 3. Five LVDT
122 sensors measure soil settlements, two of them are far from the expected interaction zone and they
123 measure the settlements due to flight and consolidation only, the other three are in line with applied
124 load, in the passive area, and can measure also the soil movement during pile loading. The pore water
125 pressure (negative and positive) in the soil is measured with three tensiometers, placed at different
126 depth at the model border. The sensor's range is -500 kPa to 500 kPa. The sensor calibration and
127 saturation procedure of the tensiometer and of the porous stone are described by Mancuso (2011).

128 The load has been applied at 35 mm from ground level by a hydraulic actuator. The loading phase
129 was displacement-controlled ($v=0.003$ mm/s at model scale), and a load cell (full scale 2500 N)
130 provided the measure of lateral load. One LVDT built in on a rotational joint gives pile's vertical
131 displacement and rotation.

132 At the end of each test, undisturbed specimen were sampled all along the model height in order
133 to obtain water content and void ratio distribution with depth.

134 MODEL PILE CHARACTERISTICS

135 The 1/100 model pile is a close-ended tube, instrumented with 10 pairs of strain gauges arranged
136 every 15 mm, Figure 4. After a calibration in the lab, the set of gauges deliver the bending moment
137 profile along the pile length. At the prototype scale ($N=100\times g$) the model represents a full circular
138 pile of 1.2 m of diameter, 15 m of embedded length with a bending stiffness of 3.9 GNm², subjected
139 to a lateral load applied at 3.5 m from ground surface. The combination of high bending stiffness
140 and relatively small slenderness ratio ($L/D = 15/1.2 = 12.5$) led to a substantial rigid behaviour of
141 the pile.

Centrifuge test and procedures

MODEL PREPARATION

The soil model used in the centrifuge model has been statically compacted in six layer, with the same procedure followed for the laboratory tests, with $w=15\%$ and $e_0=0.93$ or 0.75 and it is located on 'dry side' of the Proctor curve. The distribution of vertical compaction stresses, measured during compaction and reported in Figure 5, shows a reasonably good homogeneity for any sample and a very good repeatability of the results in different tests. The compaction stress increases with dry density from a mean value of 500 kPa in the looser state ($e_0=0.93$) to 1400 kPa in the denser state ($e_0=0.75$). The homogeneity and repeatability are confirmed also by cone penetration tests (with a $d_c=12$ mm) at $1\times g$ reported in Figure 6, referring to low compacted soil. The curves have a similar trend with an increase with depth up to $z\sim 50$ mm and then are characterized by a mean constant value of $q_c\sim 3.6$ MPa.

EXPERIMENTAL PROGRAMME

The tests performed in centrifuge are nine, four of them are presented in details, focusing the attention on two parameters: Initial void ratio (2 cases)

- Elevation of the water table (2 cases)

The testing programme is resumed in Table 4 where z_w/L is the water table elevation to embedded length ratio and e_0 , w_0 , σ_{vc} and Sr_0 are, respectively, the initial void ratio, the gravimetric water content, the compaction stress and the degree of saturation. These values have to be intended as mean values of soil properties.

PROCEDURE

In the main tests (T_06 and T_08) the pile is loaded in unsaturated conditions, until a normalized lateral displacement, y/D , of 30-40% was reached. Then, the water table z_w , has been imposed at 7 m (prototype scale) from ground level. The water table elevation over the embedded length ratio is close to 0.5 ($z_w/L = 7/15 = 0.46$).

167 In the following step, the actuator control has been switched from displacement to force control
168 and the water table level has been raised quickly to ground level. The instrumentation on the pile
169 allowed continuous monitoring of head displacement, rotation and bending moments along pile
170 during water table rising.

171 For the sake of comparison, a pile load has been conducted up to soil failure in fully saturated
172 condition, $z_p=0$ (T_05 and T_09).

173 TEST STEPS

174 The following steps characterize the main tests (T_06, T_08):

- 175 1) $1\times g$ imbibition: a zero pore pressure is applied at the model base in order to reduce after
176 compaction suction;
- 177 2) Flight and application of hydraulic condition at model base: the system has been left in
178 equalization for at least 3 hours;
- 179 3) Pile load at displacement control ($v=0.003$ mm/s);
- 180 4) Increase of water table and equalization.

181 For reference tests in fully saturated condition (T_05 and T_09), only the first three steps are
182 needed; the water table has been directly imposed at ground level.

183 **Results and discussion**

184 In this section are presented selected results to illustrate the influence of soil state condition and
185 partial saturation on the response of laterally loaded piles. The complete results of the experimental
186 program are detailed in Lalicata (2018).

187 General consideration about soil state at the end of the reference tests on saturated soil for $e_0=0.93$
188 (T_05) and $e_0=0.75$ (T_09) can be deduced by the analysis of the water content and the void ratio
189 distribution with depth reported in Figure 7. Data shows that for $e_0=0.93$ (T_05) void ratio decreases
190 with depth (typical of soil NC) from a value of ~ 0.9 at surface to a value of 0.76 for a depth of 17 m;
191 on the other hand, in T_09 ($e_0=0.75$) the void ratio is mostly constant over the entire range of depth.
192 Moreover, the comparison of the experimental data with the oedometric normal consolidation line,

193 grey line in Figure 7, highlights how the loose soil lays on the NCL below 4 meters of depth, while
 194 the denser ones intercept it at 12 meters from ground level. These differences, even for the same
 195 stress history prior to pile loading ($1\times g$ imbibition, increase of total stress and in-flight equalization),
 196 may be ascribed both on the different initial void ratio and the different shape of the WRC that
 197 controls the variation of mean effective stress and the preconsolidation pressure during hydro-
 198 mechanical stress paths (Lalicata, 2018).

199 LATERAL LOAD AT CONSTANT WATER TABLE LEVEL

200 The load-displacement curves for samples in fully saturated conditions and different void ratio
 201 are shown in Figure 8, at the prototype scale. The lateral displacement measurement, y , refers to the
 202 displacement at the load application point (nominally 3.5 m above ground level). In the range of
 203 lateral displacement explored, the load-displacement relationship is highly non-linear (Rosquoët,
 204 2007; Mayne et al., 1995, Russo, 2016).

205 The experimental data can be adequately fitted by means of a hyperbolic function (Mayne et al.,
 206 1995):

$$207 \quad H = \frac{y}{\left(\frac{1}{K} + \frac{1}{H_{lim}} y \right)} \quad (1)$$

208 Where K [MN/m] is the initial stiffness and H_{lim} [MN] is the asymptotic load. In Figure 8, the
 209 fitting of hyperbolic function with the load-test data appears to be quite satisfying: dashed and
 210 continuous lines are used for $e_0=0.75$ and 0.93 respectively. The numerical values of lateral stiffness
 211 and ultimate load are reported in Table 5.

212 The strength mobilized, under the applied lateral displacement, is different in asymptotic value
 213 and shape for denser and looser samples: for every y value, the H/H_{lim} ratio is higher for $e_0=0.93$
 214 compared to $e_0=0.75$. At the end of the test ($y=1.6$ m), for the loose soil ($e_0=0.93$, T_05) the measured
 215 load of 0.7 MN is about the 80% of ultimate capacity H_{lim} . On the contrary, the denser soil, $e_0=0.75$
 216 (T_09), is still far from the ultimate capacity showing a value of 3.2 MN for the maximum lateral
 217 displacement applied ($y=1.4$ m), giving a load ratio, H/H_{lim} , of 0.55. Initial lateral stiffness increases

218 more than three times as initial void ratio decreases as well. In addition, for low initial void ratio, the
219 load increases almost linearly for a significant displacement range, up to 0.2 m, suggesting that a small
220 amount of yielding occurs in the soil. Furthermore, in the looser state the load-displacement
221 relationship exhibits a non-linear behaviour from low values of displacement, indicating that the soil
222 develops significant plastic strain even for very low load level (Russo & Viggiani, 2009). The findings
223 are consistent with the deduced over-consolidation ratio induced by different initial void ratio already
224 commented.

225 The influence of partial saturation on the load-displacement behaviour is analysed in Figure 9,
226 where the load-displacement curves for looser (Figure 9a) and denser (Figure 9b) samples are
227 reported. In both cases, the partial saturation induces higher stiffness to the soil above the water
228 table, with more appreciable effects for high void ratio. Moreover, for loose soil in presence of partial
229 saturation the load-displacement relationship exhibits an initial linear branch, which cannot be found
230 in saturated condition, consistent with the well-known increment of preconsolidation stress in
231 unsaturated soils (Gens 2010).

232 It is known that stiffness in fine graded saturated soil depends on mean effective stress p' , void
233 ratio e and/or OCR in a non-linear way (Viggiani & Atkinson, 1995; Rampello et al., 1994). Most
234 recently other researchers have proposed a modified formulation to take into account the effect of
235 saturation degree and suction on the small strain stiffness (Biglari et al., 2011), in which stiffness
236 variations are mainly attributed both to the increase of mean effective stress p' and to increase the
237 yielding pressure induced by partial saturation (Jommi, 2000; Laloui & Nuth, 2009; Tamagnini, 2004).

238 Following the generalized effective stress framework (Laloui & Nuth, 2009; Bishop & Blight,
239 1963), in unsaturated conditions the main effective stress increases (T_{06} and T_{08}), compared to
240 saturated ones (T_{05} and T_{09}), of the quantity $\Delta p' = \gamma_w \cdot z \cdot (S_r - 1) - \gamma_w \cdot z_w \cdot S_r$. On the other hand,
241 as expected, the stiffness increment due to capillary forces, is better appreciated on the loose soil
242 ($e_0=0.93$, T_{06}) which starts from lower values of stiffness. Those increments become less important
243 as the initial structure increases due to the decreasing of initial void ratio.

244 In addition, the different distribution of saturation degree with depth for the two materials,
 245 illustrated in Figure 10, plays an important role in the understanding of the observed behaviour. For
 246 sake of simplicity, the plots are evaluated supposing that pore pressures were in hydrostatic conditions
 247 ($u = \gamma_w \cdot z_w$); the values of degree of saturation deduced from the SWRC, Table 3, are very different.
 248 At ground level, where the differences are more pronounced, the reduction of S_r compared to
 249 saturated conditions for the looser soils are 4 times higher than that corresponding to the denser soil.
 250 This difference in the distribution of S_r , give an increases in the ratio $p'_{\text{cunsat}}/p'_{\text{csat}}$ between the
 251 preconsolidation pressure in unsaturated conditions p'_{cunsat} and in saturated conditions p'_{csat} , which is
 252 properly described with a exponential function of the degree of saturation (e.g. Jommi 2000;
 253 Tamagnini 2004; Gallipoli et al 2003). As well as the stiffness and the strength increase with the
 254 decreasing of S_r .

255 Table 5 summarizes the relative influence of the position of water table, z_w/L , and soil state for
 256 lateral stiffness K and ultimate load H_{lim} respectively, evaluated by means of eq. (1). Passing from
 257 $z_w/L = 0$ to $z_w/L = 0.46$ it can be observed a stiffness increment of more than 300% for high initial
 258 void ratio and of 50% low initial void ratio. Therefore, structure effects induced by partial saturation
 259 are significantly important for soil with initial open structure because of lower values of saturation
 260 degree which allows developing higher bonding effect induced by meniscus. A direct connection
 261 between lateral stiffness K and soil stiffness E_s cannot be easily recognised because of the pile behaves
 262 almost like a rigid pile, hence the head displacement is the sum of a deflection and a rigid rotation
 263 (Lalicata, 2018) and elastic solutions (Randolph 1981, Higgins et al. 2013, Di Laora and Rovithis
 264 2015) are not directly applicable. In comparison with lateral stiffness, H_{lim} appears to be less affected
 265 by partial saturation: compared to saturated condition, gains are 12% for $e_0 = 0.75$ and 220% for $e_0 =$
 266 0.93.

267 The comparison of bending moment profiles, at 0.1 MN of applied load, for T_08 and T_09 (e_0
 268 = 0.75) is presented in Figure 11 (a). The pile does not behaves as a purely flexible pile, since bending
 269 moment propagates all along the entire embedded length then the active length of the pile is equal,
 270 or even greater of, to the actual length L (Randolph, 1981). The stiffness increment in the shallower

271 seven meters from ground level, induced by partial saturation, led to a reduction of maximum bending
272 moment of more than 20% for $H=0.1$ MN. Thanks to partial saturation, the position of maximum
273 bending moment slightly moves upward passing from 5 to 4 meter from mudline. The small
274 differences of the moment measured at the ground level in the two cases may be ascribed to the
275 different settlement of the soil during the consolidation phase (Lalicata, 2018).

276 Double derivation of moment profile allows calculating the soil pressure distribution along the
277 pile for every load increment. Soil pressure distribution is shown in Figure 11 (b) for the same soil
278 condition and load level of Figure 11 (a). In the shallower part, the unsaturated soil hold higher
279 pressure compared to the saturated one. Pressure remains almost constant in the first 6 meters from
280 ground level and then it reduces smoothly towards the pile tips changing sign at 12 meter of depth.

281 Referring to almost rigid piles, the findings reported in the present study seems to indicate that
282 the unsaturated zone above water table can change significantly the soil reactions distribution all
283 along the pile length.

284 The ratio of maximum bending moment obtained for unsaturated condition and saturated
285 condition remains at the constant value of 0.76 for relatively low lateral load, up to 0.5 MN, then it
286 gradually increases to 0.94 measured for $H=2.1$ MN, as with the increase of the applied load the rigid
287 behaviour becomes dominant compared to the flexural one in both cases (Figure 12).

288 The bending moment profiles of T_06 and T_08, relative to 0.1 MN of lateral load, are pointed
289 out in Figure 13. This comparison allows to highlight the influence of soil stiffness, here mainly
290 related to initial void ratio and different S_v distribution, on bending response of the pile: as for softer
291 soil (T_06, $e_0 = 0.93$) the interaction involves greater volumes of soil compared to stiffer ones (T_08,
292 $e_0 = 0.75$). As expected, the bending moment increases as soil stiffness decreases, and as for the looser
293 sample (T_06), the bending moment distribution is more homogeneous along the entire pile length
294 and the maximum bending moment takes place at greater depth. It is worth noting that all these
295 results are significantly affected by the moment at ground level induced by load eccentricity that
296 significantly increases the values of the maximum bending moment and the downward load transfer
297 (Budhu & Davies, 1987).

298

WATER TABLE RISING AT CONSTANT LOAD

299 For T_06 and T_08, when the lateral head displacement has reached the 30-40% of the diameter,
300 the loading phase has been stopped and the actuator has been switched from displacement control
301 to loading control. By the electro-pneumatic valves system, the pore pressure at the bottom of the
302 model has been raised quickly from 120 kPa to 190 kPa, in order to simulate the water table raising
303 from 7 m of depth to 0 m. The model has been left in equalization for the remaining time test (320
304 min for T_06 and 380 min for T_08, at model scale), the analysis of soil settlements and pore pressure
305 evolution indicates that the stationary condition has not been reached in none of the tests (Lalicata,
306 2018).

307 Suction decreases, due to imbibition, led to a reduction of mean effective stress and of the
308 preconsolidation pressure (where the collapse for saturation occurs), as well as of the soil stiffness
309 and strength. As a result, the pile head displacement has increased in both tests (Figure 14).
310 Displacement increment resulted higher for open soil structure, T_06, than for closer one, T_08. The
311 global response reported in Figure 14 (a) and (b) is the result of a combination of multiple factors
312 such as differences in saturated permeability, different soil stiffness prior to loading and load ratio
313 level between initial load and ultimate load in saturated condition. First, since saturated permeability
314 decreases with void ratio and, in this phase, the hydraulic equilibrium was far to be reached, lower
315 values of pile lateral displacement are expected for the model with $e_0=0.75$. Secondly, for the same
316 perturbation applied, higher displacement is expected for loose soil ($e_0=0.93$) because of lower
317 stiffness. Finally, looking at the comparison between the load-displacement relationship for saturated
318 and unsaturated condition, it seems reasonable to suppose that for $e_0=0.93$ (Figure 14 (a)) a lateral
319 load of 1.2 MN it is not sustainable in fully saturated conditions; while, for $e_0=0.75$ even with no
320 suction (Figure 14 (b)), a value of 2.1 MN appears to be sustainable by soil, then the system could
321 have advanced faster to collapse in the first case. However, it is to be noted that the load-deflection
322 curve obtained in saturated conditions (i.e. T_09) not necessarily represents a lower bound solution,
323 given that soil behaviour is strongly nonlinear and dissipative, therefore the final point measured
324 during saturation (grey triangles in Figure 14 (b)) did not represent the end of the process.

325 The evolution of head displacement with the centrifuge time and the pore pressure for the two
326 tests are presented in Figure 15 (a) and (b). In both Figures, black line refers to $e_0=0.93$ (T_06), grey
327 colour is used for $e_0=0.75$ (T_08); in Figure 15 (b) different tensiometers position with depth is
328 illustrated with various style line: a continuous line has been used for $z=4\text{m}$, large dashes for $z=9\text{m}$
329 and, finally, small dashes has been used for $z=14\text{m}$. In order to better emphasize the phenomena, the
330 results are represented in a semi-logarithmic plane and time has been replaced to zero just before the
331 increase of water pressure. Instead of elapsed time, the Terzaghi non-dimensional formulation for
332 time factor has been used: $T = \frac{c_v}{H^2}t$, where c_v is the coefficient of vertical consolidation, t is the
333 elapsed time and H is the drainage layer. For sake of simplicity the same reference values of c_v and H
334 are adopted for all the tests and are $1.0 \times 10^{-6} \text{ m}^2/\text{s}$ (Table 2) and 180 mm (initial soil model height)
335 respectively. It is interesting to note that, even if no stabilization occurs, the slope of the pore pressure
336 curves gradually reduces, while the increment of lateral displacement keeps growing; moreover, in
337 the last part of the test, a slight increment of displacement rate can be observed for T_06.

338 During saturation, the strength reduction in upper part produced the reduction of soil pressure
339 against the pile in the first meters of depth from ground level and an increase in the last meters.
340 Observing the bending moment profiles prior and post water table rising, it can be observed (Figure
341 16) a general increment of the moment below the position of the maximum bending moment (from
342 6 m to 15 m of depth). Since the pile undergoes a rigid body motion during saturation the maximum
343 bending moment variation is less than 10%.

344 **Conclusion**

345 In the present work, the soil pile interaction under lateral loading in unsaturated condition, by
346 means of centrifuge tests has been studied. The models have been statically compacted at two
347 different void ratios and the same water content. The initial conditions have been chosen based on a
348 wide set of flooding tests at different void ratios and water content with the aims to cover a range of
349 void ratios representative of *in situ* soil conditions.

350 The pile has been loaded with two positions of water table: one at half of pile's embedded length
351 ($z_w = 7$ m) and the other at ground level ($z_w = 0$ m). Compared to saturated conditions, a significant
352 increase in lateral stiffness on the load-deflection relationship: 300% for loose soil ($e_0=0.93$) and 50%
353 for dense soil ($e_0=0.75$) has been observed in both cases. The effect of partial saturation is stronger
354 for the looser state as, for the same suction, bonding effects due to capillary forces gives a major
355 increment in soil structure. Moreover, the major changes of S_r in the looser sample is given to the
356 different shape of WRC with void ratio.

357 The present study focus on the behaviour of an almost rigid pile and additional tests are required
358 to investigate the effect of partial saturation varying the soil-pile relative stiffness and the slenderness
359 ratio. In the particular case of rigid pile, that involves a significant volume proportional to the entire
360 embedded length, the increase of soil stiffness in the shallower soil layer leads to a reduction of
361 maximum bending moment more than 20% that moves towards ground surface. For flexible piles
362 that have a critical length lower than the embedded length, the pile response is strongly dependent
363 from the stiffness of the soil close to the surface. Therefore, it is possible that stiffness variation
364 induced by partial saturation may will have more visible effects for flexible piles compared to the
365 rigid pile of this study, which represents a lower bound solution in the understanding of the role of
366 partial saturation in horizontally loaded piles

367 During saturation, due to the combination of excessive load level and strong variation of water
368 table level, the system goes towards soil collapse with a close to rigid body motion. Findings appear
369 to show that neglecting the presence of partial saturation is not necessarily a safety solution when
370 significant variation of saturation degree takes place. Reduction of soil strength and stiffness due to
371 saturation can lead to greater pile head displacement than those predicted by fully saturated analysis.
372 The increase of lateral displacement depends both on of the value of the load and the initial water
373 table position.

374 **Acknowledgments**

375 This research has been performed in the framework of the GEO-TRANSALP-PILE-UNSAT
376 agreement developed between DISG, the "Department of Structural and Geotechnical Engineering"

377 of "Sapienza" University of Rome, "Department of Department of Civil and Computer Engineering"
378 University of Rome "Tor Vergata" and IFSTTAR, the "French Institute of Science and Technology
379 for Transport, Development and Networks". They are greatly acknowledged. The authors would like
380 to thank the technical team of the Ifsttar's geo-centrifuge, the technical staff of DISG geotechnical
381 laboratory and also Dr. M. Blanc for his advices.

382 **References**

383 Banerjee P.K., Davies T.G. (1978). The behaviour of axially and laterally loaded single piles
384 embedded in nonhomogeneous soils. *Géotechnique*, 28 (3), 309 – 326.

385 Biglari, M., Mancuso, C., d'Onofrio, A., Jafari, M. K., Shafiee, A. Modelling the initial shear
386 stiffness of unsaturated soils as a function of the coupled effects of the void ratio and the degree of
387 saturation. *Computers and Geotechnics*, 38 (2011) 709–720.

388 Bishop, A., Blight, G., (1963). Some aspects of effective stress in saturated and partly saturated
389 soils. *Géotechnique* 13, 177–197.

390 Budhu M., Davies T.G. (1987). Nonlinear analysis of laterally loaded piles in cohesionless soils.
391 *Can. Geotech. J.*, 24 (2), 289 – 296.

392 Caicedo, B., Medina, C., Cacique, A. (2006). Validation of time scale factor of expansive soils in
393 centrifuge modeling. *Physical modeling in Geotechnics ICPMG06*, Ng, Zhang, Wang (eds), 273–277.

394 Caicedo, B., Thorel, L. (2014). Centrifuge Modelling of Unsaturated soils. *Special Issue « Advances
395 in the Mechanics of Unsaturated soils » of the Journal of Geoengineering Sciences*. Vol.2,n°1-2, 83-103 (july 2014)
396 DOI 10.3233/JGS-130013.

397 Casini, F., (2008). Effetti del grado di saturazione sul comportamento meccanico di un limo. *Ph.D.
398 thesis*, Università degli studi di Roma La Sapienza.

399 Casini, F., Vaunat, J., Romero, E., Desideri, A., (2012). Consequences on water retention
400 properties of double-porosity features in a compacted silt. *Acta Geotechnica* (2012) 7:139–150.

401 Corté J.F. (1989) Model testing-Geotechnical model tests, *Proc. XII ICSMFE Rio*, 2553-2571.

402 Cui, Y., Delage, P., (1996). Yielding and plastic behaviour of an unsaturated compacted silt.
403 *Géotechnique*, 46 (2), 291–311.

404 Depountis N, Davies MCR, Harris C, Burkhart S, Thorel L, Rezzoug A, Konig D, Merrifield C,
405 Craig WH. Centrifuge modelling of capillary rise, *Engineering Geology*, 2001;60(1-4):95-106. ISSN:
406 0013-7952 .

407 Di Laora, R., Rovithis, E. (2015). Kinematic Bending of Fixed-Head Piles in Nonhomogeneous
408 Soil. *J. Geotech. and Geoviron. Eng.* No141.

409 Escario, V., Saez, J., (1986). The shear strength of partly saturated soils. *Géotechnique*, 36 (3), 453–
410 456.

- 411 Fredlund, D.G., Xing A., (1994). Equation for the soil-water characteristic curve. *Can. Geotech. J.*
412 31 (4), 521–532.
- 413 Gens, A., (2010). Soil–environment interactions in geotechnical engineering. *Géotechnique*, 60 (1),
414 3–64.
- 415 Gens, A., Alonso, E. E., Surlol, J., Lloret, A. (1996). Effect of structure on the volumetric
416 behaviour of a compacted soil. *Proc. 3rd Int. Conf.on Unsaturated Soils, Paris 1*, 83-88.
- 417 Georgiadis K., Potts D.M. & Zradkovic L. (2003). The influence of partial saturation on pile
418 behavior. *Géotechnique*, 53 (1), 11 – 25.
- 419 Higgins, W., Vasquez, C., Basu, D., Griffiths, D.V. (2013). Elastic solution for laterally loaded
420 piles. *Journal of Geotechnical and Geoenvironmental Engineering*. No 139, 1096-1103.
- 421 Jommi, C. (2000). Remarks on the constitutive modelling of unsaturated soils. *Proc. Experimental*
422 *Evidence and theoretical Approaches in Unsaturated Soils*, Tarantino & Mancuso (eds), Balkema, Rotterdam,
423 139-153.
- 424 Khemakhem, M., Chenaf, N., Garnier, J., Rault, G., Thorel, L., Dano, C. Static and cyclic lateral
425 pile behavior in clay. *7th International Conference on Physical Modelling in Geotechnics 2010*, ICPMG
426 2010Volume 2, 2010, Pages 953-958.
- 427 Krishnan R., Gazetas G., Velez A. (1983). Static and dynamic lateral deflexion of piles in non –
428 homogeneous soil stratum. *Géotechnique*, 33 (3), 307 – 325.
- 429 Lalicata, L. 2018. Effect of saturation degree on the mechanical behaviour of a single pile
430 subjected to lateral forces (in Italian). *Ph.D Thesis*, Sapienza Università di Roma.
- 431 Laloui, L., Nuth, M. (2009). On the use of the generalised effective stress in the constitutive
432 modelling of unsaturated soils. *Comp and Geotech.* 36, 20-23.
- 433 Mancuso, C. et al. (2011) . Messa a punto di un nuovo minitensiometro ad alta capacità. *LARG*.
- 434 Mayne, P.W., Kulhawy, F. H., Trautmann, C. H., (1995). Laboratory Modeling of Laterally-
435 Loaded Drilled Shafts in Clay. *J. Geotech. Eng.*, 1995, 121(12): 827-835.
- 436 Rampello, S., Silvestri, F. & Viggiani G. (1994b). The dependence of G_0 on stress state and history
437 in cohesive soils. *Proc. 1st Int. Conf. Pre-failure Deform. Character. Geomater.*, Sapporo 2, 1155-1160.
- 438 Randolph M.F. (1981). The response of flexible piles to lateral loading. *Géotechnique*, 31 (2), 247 –
439 259.
- 440 Romero, E., (1999). Characterization and thermo-hydro-mechanical behaviour of unsaturated
441 Boom clay: an experimental study. *Ph.D. thesis*. Universitat Politècnica de Catalunya Barcelona, Spain.
- 442 Romero, E., Della Vecchia, G., Jommi, C. (2011). An insight into the water retention properties
443 of compacted clayey soils. *Géotechnique* 61, (4), 313–328.
- 444 Romero, E., Lloret, A., Gens, A., (1995). Development of a new suction temperature controlled
445 oedometer cell. In: Alonso, E., Delage, P. (Eds.), *1st Int. Conf. on Unsaturated Soils*, Paris. Balkema.

- 446 Romero, E., Vaunat, J., (2000). *Retention curves of deformable clays*. Proc. Experimental Evidence and
 447 theoretical Approaches in Unsaturated Soils, Tarantino & Mancuso (eds), Balkema, Rotterdam, 90-
 448 106.
- 449 Rosquoët, F., Thorel, L., Garnier, J., Canepa, Y. 2007. Lateral cyclic loading of sand-installed piles.
 450 *Soils and Foundations* 47(5), 821-832.
- 451 Russo, G. (2016). A method to compute the non-linear behavior of piles under horizontal loading.
 452 *Soils and Foundation*. 56 (1), 33-43.
- 453 Russo, G., Viggiani, C. (2009). Piles under horizontal load: an overview. *Proceedings of the Second*
 454 *BGA International Conference on Foundations*, ICOF2008. Brown M. J., Bransby M. F., Brennan A. J. and
 455 Knappett J. A. (Editors).
- 456 Salager, S., Nuth, M., Ferrari, A., Laloui, L., (20013). Investigation into water retention behaviour
 457 of deformable soils. *Can. Geotech. J.* (50), 200–208.
- 458 Schofield, A. N. (1980). Cambridge geotechnical centrifuge operation. *Geotechnique* 30, No. 1, 229–
 459 267, <http://dx.doi.org/10.1680/geot.1980.30.3.227>
- 460 Sivakumar, V., Wheeler, S. J., (2000). Influence of compaction procedure on the mechanical
 461 behavior of an unsaturated compacted clay Part 1: Wetting and isotropic compression. *Geotechnique*,
 462 50 (4), 359–568.
- 463 Soranzo, E., Tamagnini, R., and Wu, W. 2015. Face stability of shallow tunnels in partially
 464 saturated soil: centrifuge testing and numerical analysis. *Géotechnique*, 65(6): 454–467.
- 465 Tamagnini, R., (2004). An extended cam-clay model for unsaturated soils with hydraulic
 466 hysteresis. *Géotechnique* 54, 223–228.
- 467 Tarantino, A. & De Col, E. (2008). Compaction behaviour of clay. *Géotechnique* 58, No. 3, 199–
 468 213.
- 469 Thorel, L. et al. (2011). Physical modelling of wetting-induced collapse in embankment base.
 470 *Geotechnique* 61 (5), 409–420.
- 471 Van Genuchten, M. T., 1980. A closed-form equation for predicting the hydraulic conductivity of
 472 unsaturated soils. *Soil Sci. Soc. Am.* 44 (1), 892–898.
- 473 Vanapalli, S.K. (2009). Shear strength of unsaturated soils and its applications in geotechnical
 474 engineering practice. *Keynote lecture, Proc., 4th Asia-Pacific Conference on Unsaturated Soils*, Newcastle, 579-
 475 598.
- 476 Vassallo, R., Mancuso, C., Vinale, F., (2007). Effects of net stresses and suction history on the
 477 small strain stiffness of a compacted clayey silt. *Can. Geotech. J.* 44 (4), 447–462.
- 478 Viggiani, G. & Atkinson, J. H., (1995). Stiffness of fine-graded soils at very small strains.
 479 *Géotechnique* 45, (2), 249-265.
- 480 Wheeler, S. J., Sivakumar, V., (1995). An elasto–plastic critical state framework for unsaturated
 481 soil. *Geotechnique*, 45 (1), 35–53.

Table 1: Scaling laws for centrifuge modelling.

Parameter	Scaling law model/prototype
Length	$1/N$
Density	1
Unit weight	N
Stress	1
Strain	1
Force	$1/N^2$
Bending moment	$1/N^3$
Seepage velocity	$1/N$
Consolidation time	$1/N^2$
Capillary rise	$1/N$

483

Table 2: Index properties and hydro-mechanical properties of B-Grade kaolin.

w _L (%)	w _P (%)	IP (%)	ρ_s (gr/cm ³)	C_C (-)	C_S (-)	N_0 (-)	ϕ' (°)	k_{sat} (m/s)	c_v (m ² /s)
42.2	28.2	14.0	2.66	0.26	0.078	1.36	22	4.0·10 ⁻⁹	1.0·10 ⁻⁶

484

Table 3: Van Genuchten parameters for different void ratio.

e_0	$S_{r_{sat}}$	$S_{r_{res}}$	α	n	m
(-)	(-)	(-)	(1/kPa)	(-)	(1-1/n)
0.93	1.0	0.16	0.02	1.4	0.2501
0.75	1.0	0.16	0.006	1.3	0.2307

485

Table 4: Testing programme.

Name	e_0 (-)	z_w/L (-)	w_0 (%)	σ_v (kPa)	Sr_0 (%)
Test 05 T_05	0.93	0.0	15.03	580	42.02
Test 06 T_06	0.93	0.46	14.67	559	41.01
Test 08 T_08	0.75	0.46	14.72	1395	51.03
Test 09 T_09	0.75	0.0	14.72	1395	51.03

486

Table 5: Lateral stiffness and asymptotic load.

Test	z_w/L (-)	K (MN/m)	H_{lim} (MN)	e_0 (-)
T_05	0.0	1.5	0.9	0.93
T_06	0.46	6.2	2.9	0.93
T_09	0.0	5.0	5.6	0.75
T_08	0.46	7.4	6.3	0.75

487

C_c	(-)	slope of normalconsolidation line (NCL) in 1D
C_s	(-)	slope of unloading-reloading line (NCL) in 1D
c_v	(m ² /s)	coefficient of vertical consolidation
D	(m)	pile diameter
e	(m)	eccentricity of lateral load
e, e_0, e_{opt}	(-)	void ratio, initial void ratio, optimum void ratio
E_s	(MPa)	soil stiffness
g	(m/s ²)	gravitational acceleration
H, H_{lim}	(MN)	lateral load, asymptotic lateral load
IP	(%)	plastic index
K	(MN/m)	initial lateral stiffness
k_{sat}	(m/s)	saturated permeability
L	(m)	embedded pile length
m	(-)	Van Genuchten parameter
M, M_{sat}	(MNm)	bending moment, maximum bending moment in saturated condition
N	(-)	scaling factor
n	(-)	Van Genuchten parameter
N_0	(-)	reference void ratio on the NCL_1D at $\sigma'_v=1$ kPa
OCR	(-)	over consolidation ratio
p'	(kPa)	mean effective stress
q_c	(MPa)	cone resistance of CPT test
s	(kPa)	matrix suction
S_r, S_{r0}	(-)	saturation degree, initial saturation degree
$S_{r_{sat}}, S_{r_{res}}$		saturated saturation degree, residual saturation degree
u_w	(kPa)	pore water pressure
v	(mm/s)	compaction rate
v	(mm/s)	lateral displacement rate
w, w_0, w_{opt}	(-)	gravimetric water content, initial gravimetric water content, optimum gravimetric water content
w_L	(%)	liquid limit
w_L	(%)	plastic limit
y	(m)	lateral displacement at the application point
z	(m)	depth
z_w	(m)	water table position
α	(1/kPa)	Van Genuchten parameter
$\gamma_{d,opt}$	(kg/cm ³)	optimum dry density
γ_s	(kN/m ³)	unit weight of solids
γ_w	(kN/m ³)	unit weight of water
φ'	(°)	friction angle

490 **Figure 1: Flooding test results in the compaction plane.**

491 **Figure 2: Main wetting Soil Water Retention curves for B-grade Kaolin.**

492 **Figure 3: Experimental set-up and instrumentation.**

493 **Figure 4: Model pile instrumented with 10 pairs of strain gauges.**

494 **Figure 5: Vertical compaction stress with depth for different models.**

495 **Figure 6: CPT profiles for $e_0=0.93$.**

496 **Figure 7: Water content and void ratio with depth after test T_05 and T_09.**

497 **Figure 8: Effect of soil state condition on Lateral Load-Displacement curves (prototype scale).**

498 **Figure 9: Load-displacement curves for (a) loose soil ($e_0=0.93$); (b) dense soil ($e_0=0.75$).**

499 **Figure 10: Different distribution of saturation degree due to different porosity.**

500 **Figure 11: Comparison of bending moment distribution along pile for highly compacted soil for $z_w/L=0$ (T_09) and z_w/L**
501 **$=0.46$ (T_08).**

502 **Figure 12: Maximum bending moment ratio, in unsaturated and saturation condition, for highly compacted soil, $e_0=0.75$.**

503 **Figure 13: Comparison of bending moment distribution along pile for $z_w/L=0.46$ and different initial void ratio.**

504 **Figure 14: Load-displacement curves during saturation for (a) loose soil ($e_0=0.93$); (b) dense soil ($e_0=0.75$).**

505 **Figure 15: Evolution with time during rising table of tests T_06 and T_08: a) lateral displacement; b) pore pressure at different**
506 **depth.**

507 **Figure 16: Bending moment profiles after and before saturation for a) $e_0=0.93$; b) $e_0=0.75$.**

508

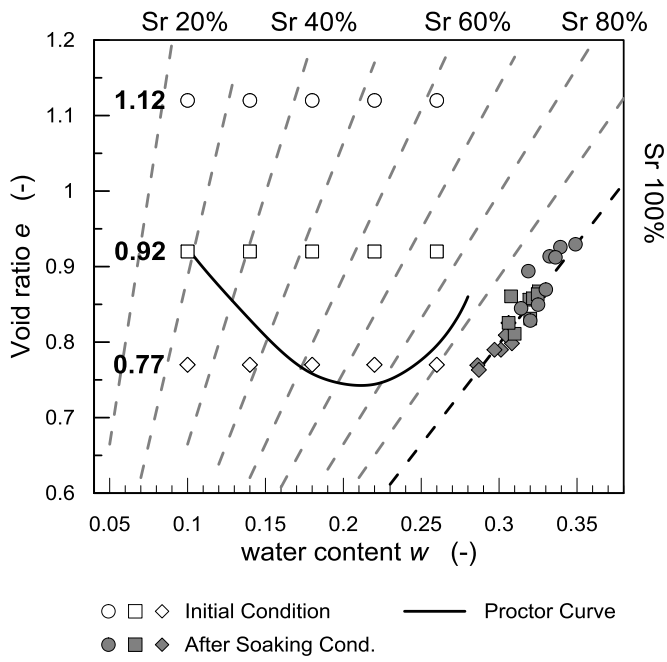


Figure 1: Flooding test results in the compaction plane.

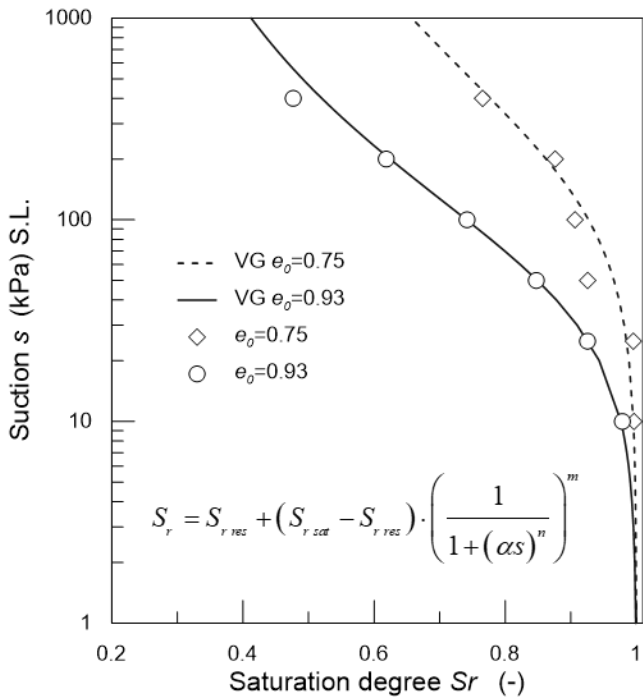


Figure 2: Main wetting Soil Water Retention curves for B-grade Kaolin.

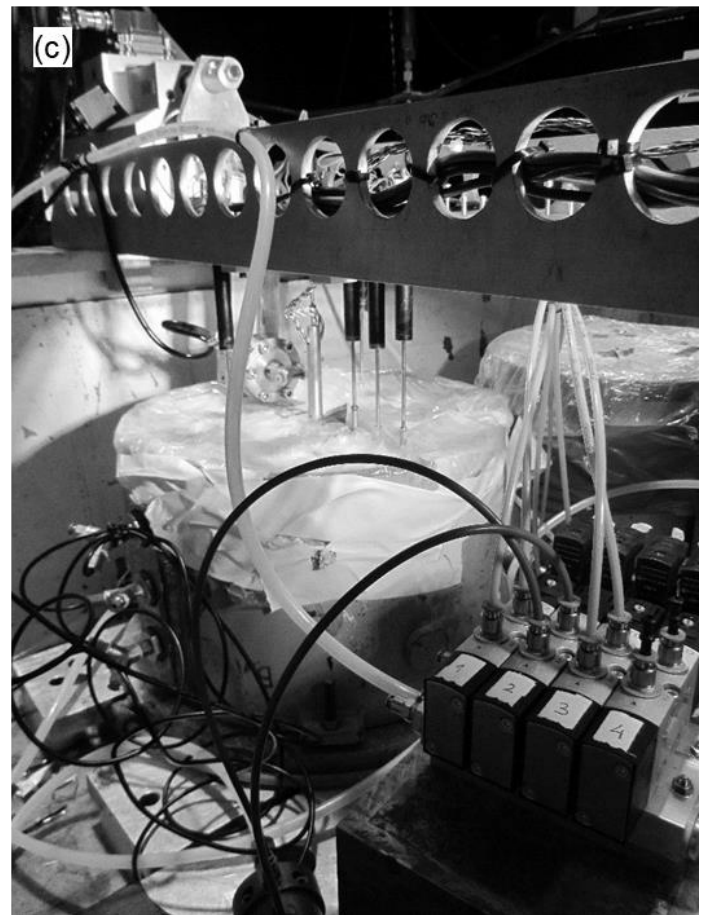
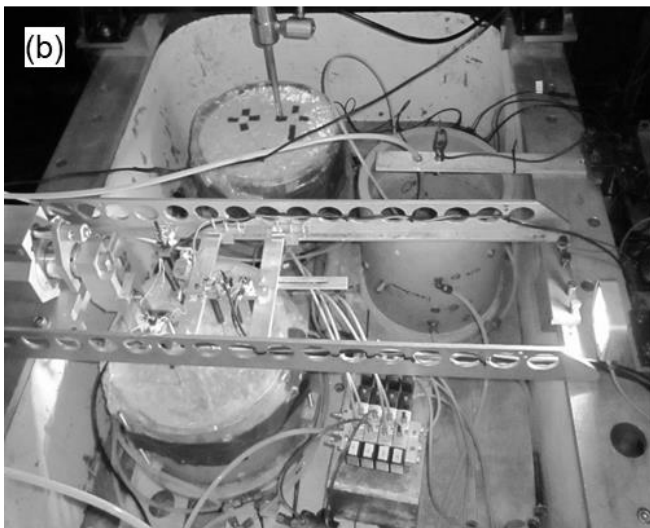
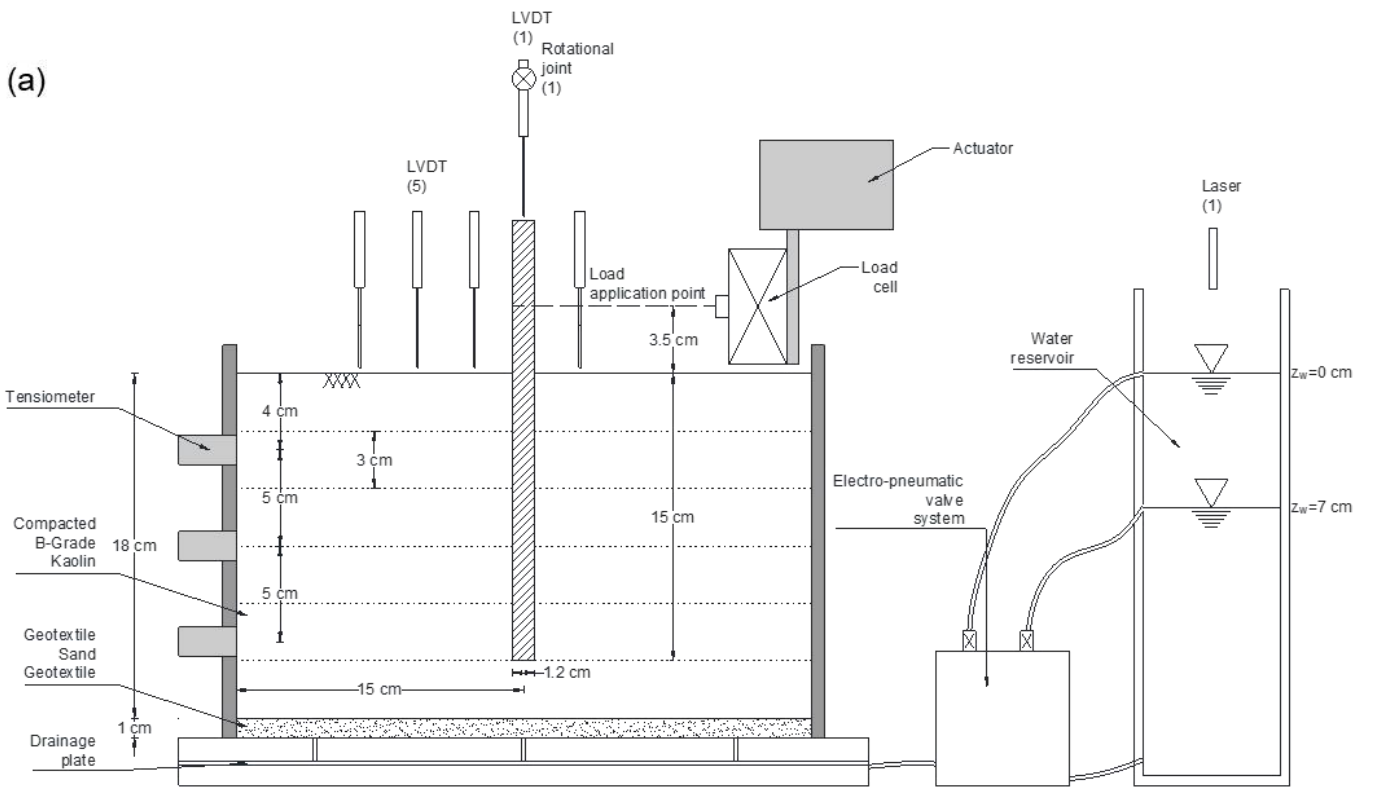


Figure 3: Experimental model: (a) cross section in the load plane, (b) aerial view of the basket, (c) perspective of valve system and soil container, (d) detail of the loading system and LVDT.

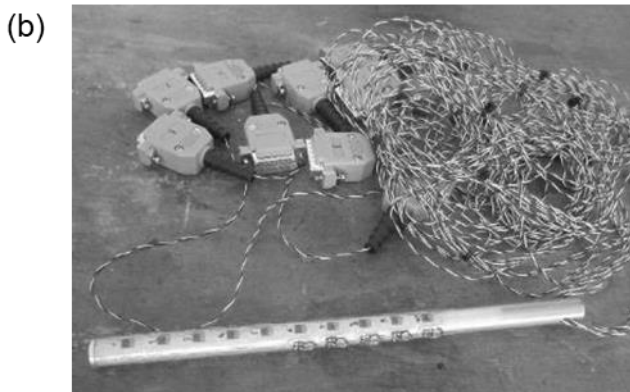
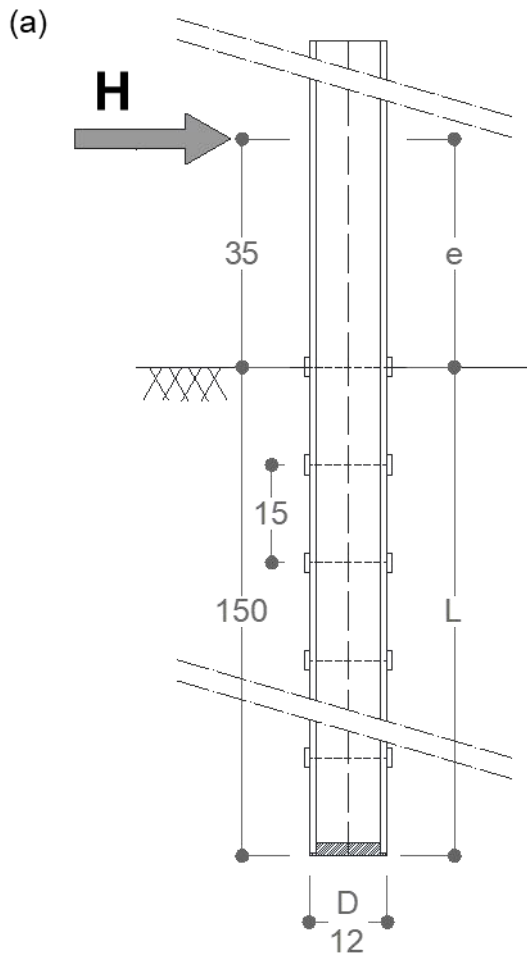
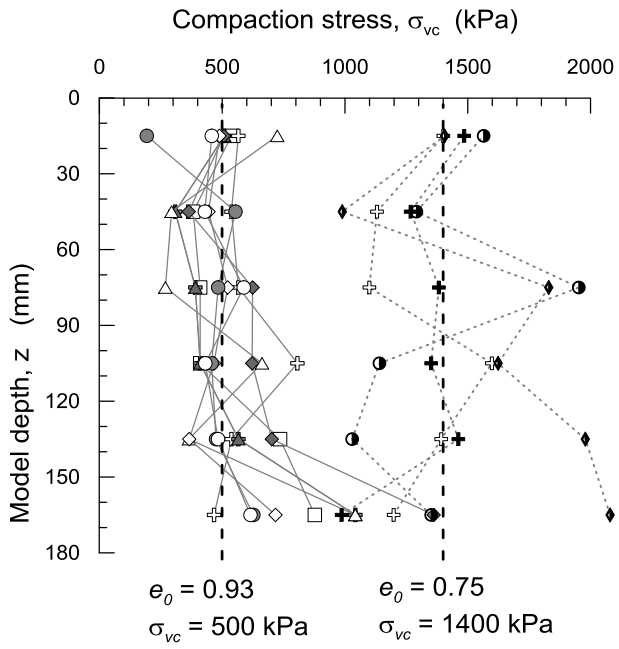


Figure 4: Instrumented model pile: (a) schematic cross section, (b) general view.

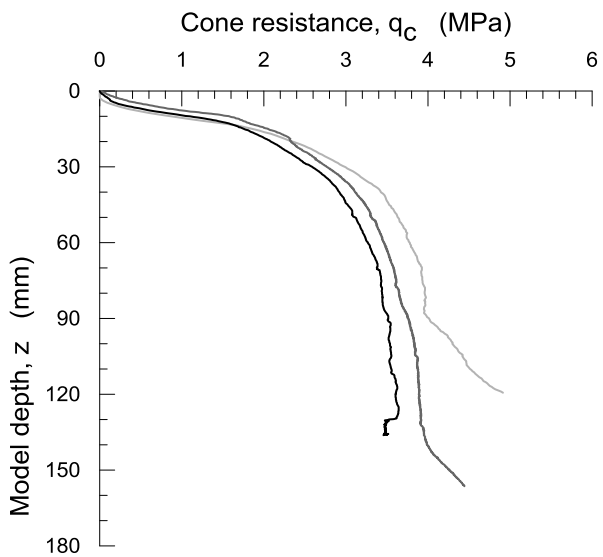


521

522

Figure 5: Vertical compaction stress with depth for different models, each point is located in the middle of one layer.

523



524

525

Figure 6: CPT profiles for $e_0=0.93$.

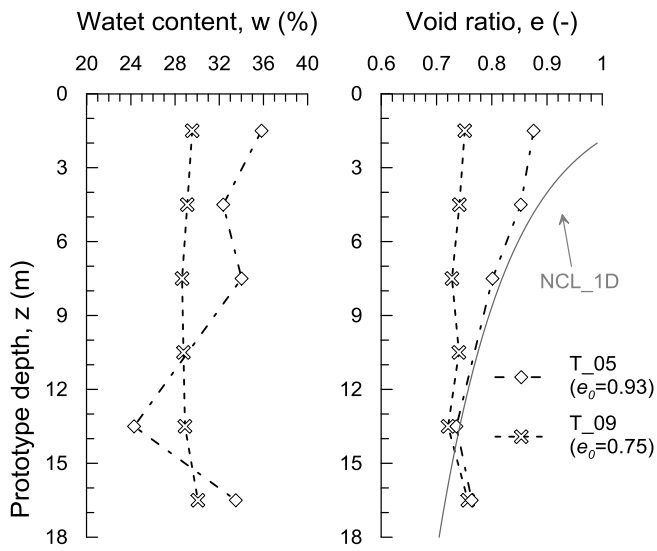


Figure 7: Mean values of water content and void ratio with depth after tests T_05 ($e_0=0.93$) and T_09 ($e_0=0.75$).

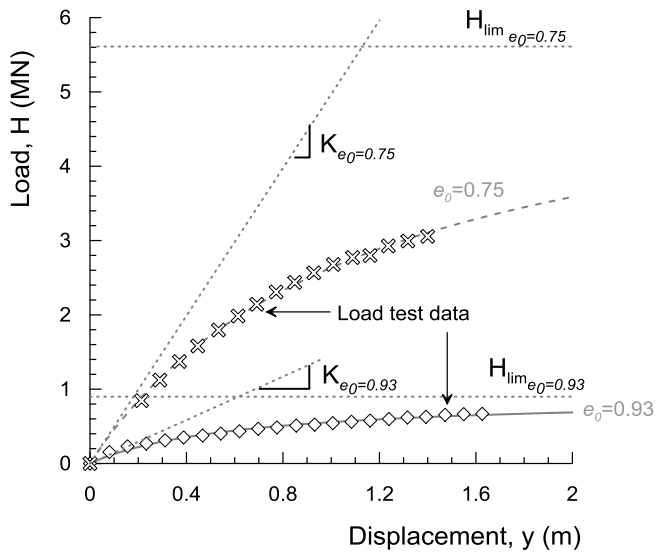


Figure 8: Effect of soil state condition on Lateral Load-Displacement curves (prototype scale).

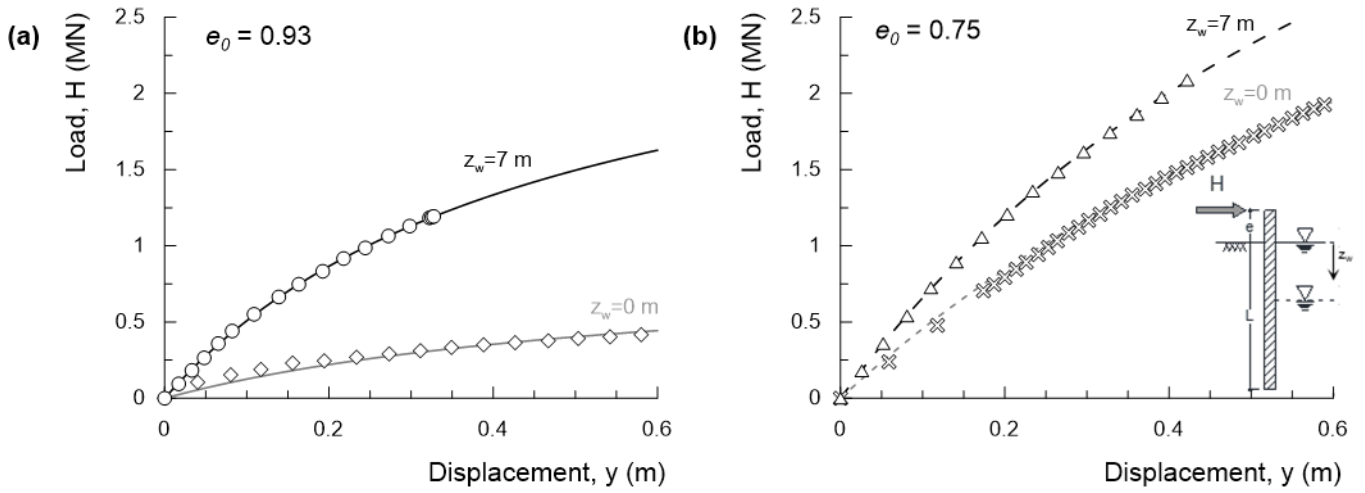


Figure 9: Load-displacement curves: (a) loose soil ($e_0=0.93$), (b) dense soil ($e_0=0.75$).

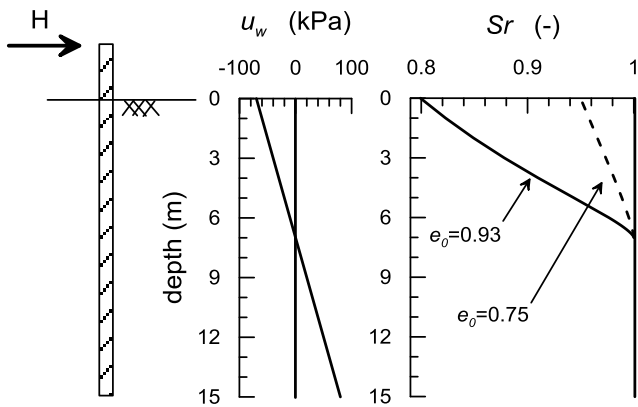


Figure 10: Different distribution of saturation degree due to different porosity for $z_w=7$ m.

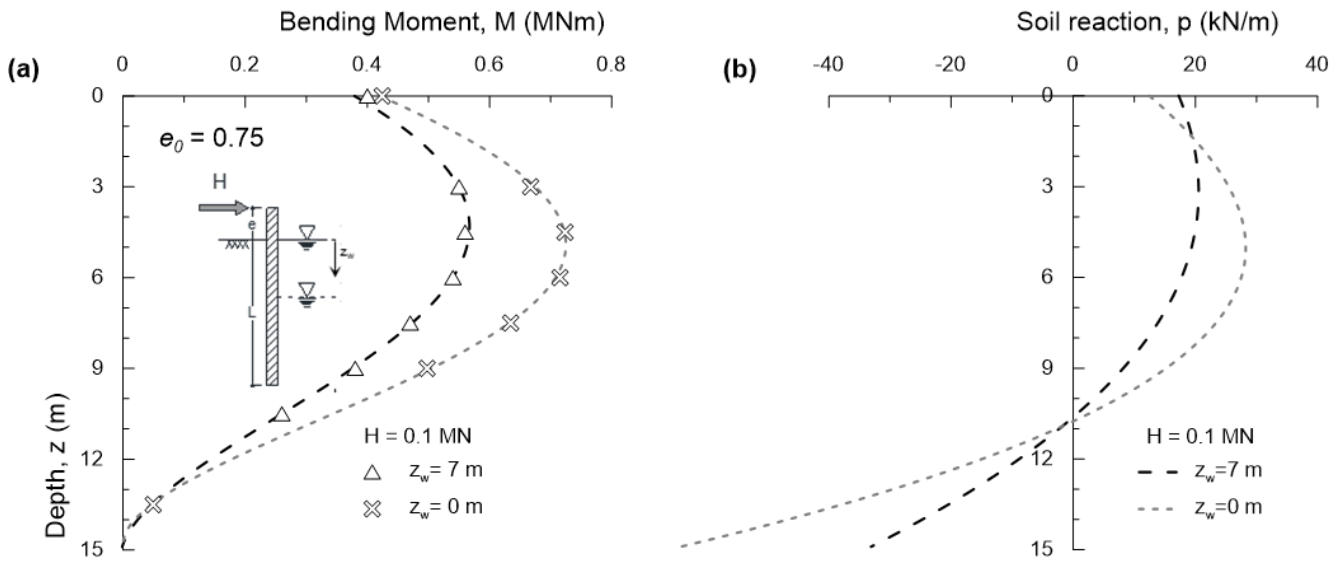
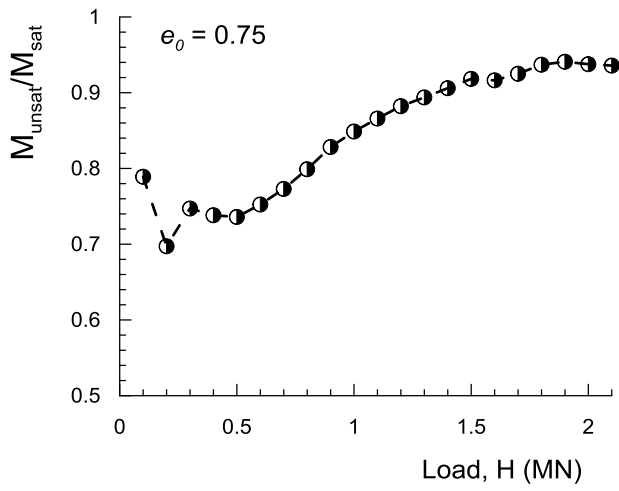


Figure 11: Influence of water table elevation, $z_w = 0$ (T_09) and $z_w = 7$ m (T_08), for highly compacted soil ($e_0=0.75$): (a) bending moment distribution along pile, (b) soil reaction distribution along pile.

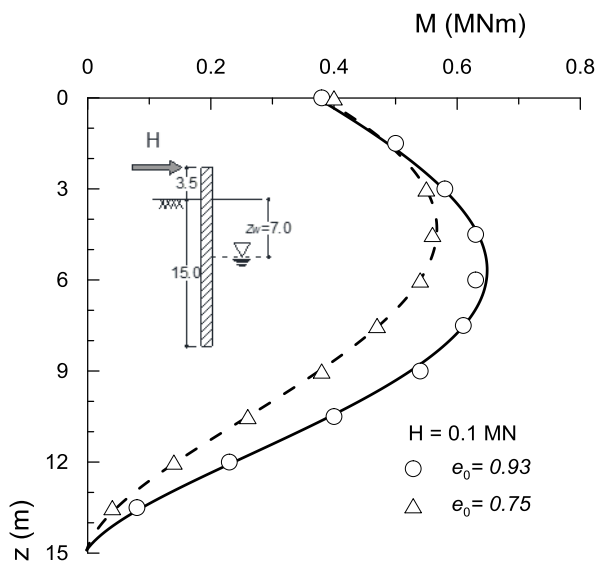


541

542

Figure 12: Maximum bending moment ratio, in unsaturated and saturation condition, for highly compacted soil, $e_0=0.75$.

543



544

545

Figure 13: Comparison of bending moment distribution along pile for $z_w = 7$ m and different initial void ratio.

546

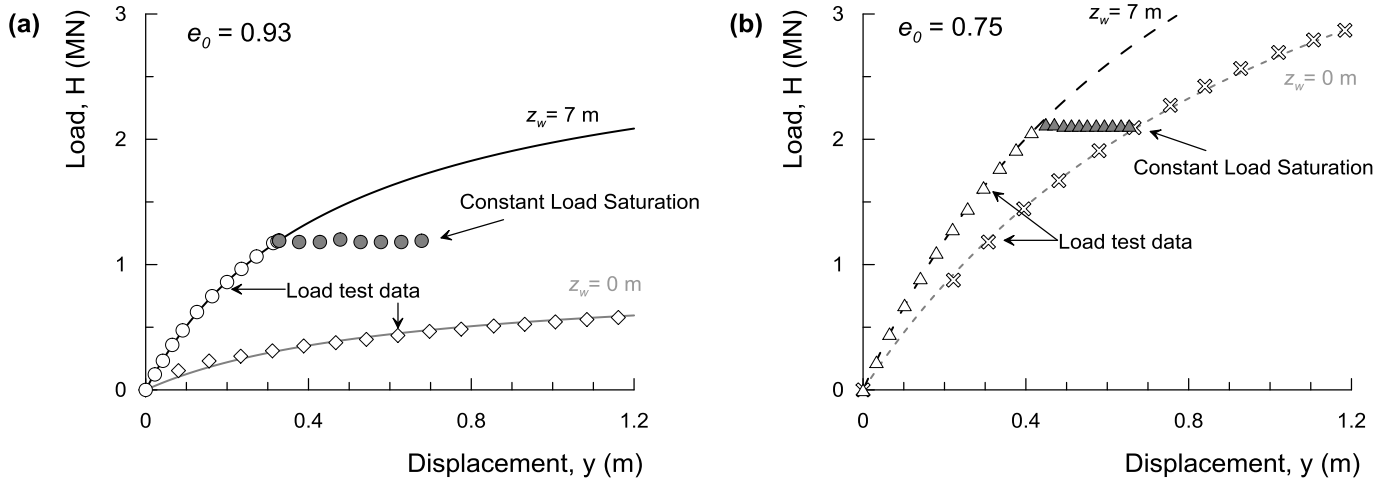


Figure 14: Load-displacement curves during saturation: (a) loose soil ($e_0=0.93$), (b) dense soil ($e_0=0.75$).

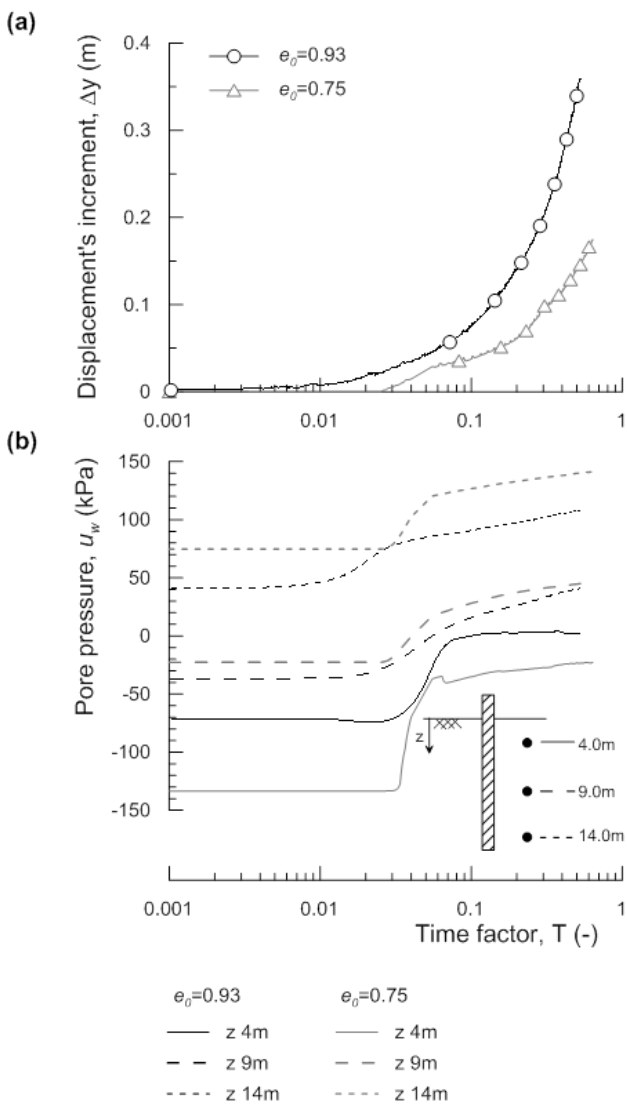


Figure 15: Evolution with time during water table rising of tests T_06 ($e_0=0.93$) and T_08 ($e_0=0.75$): (a) lateral displacement, (b) pore pressure at different elevations.

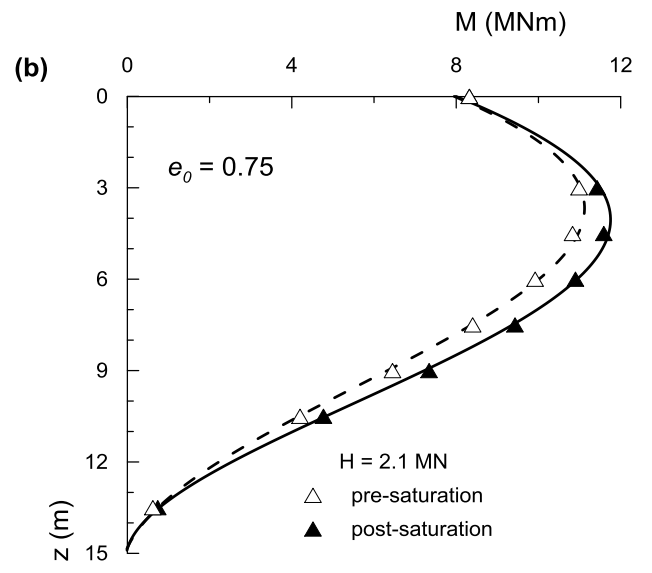
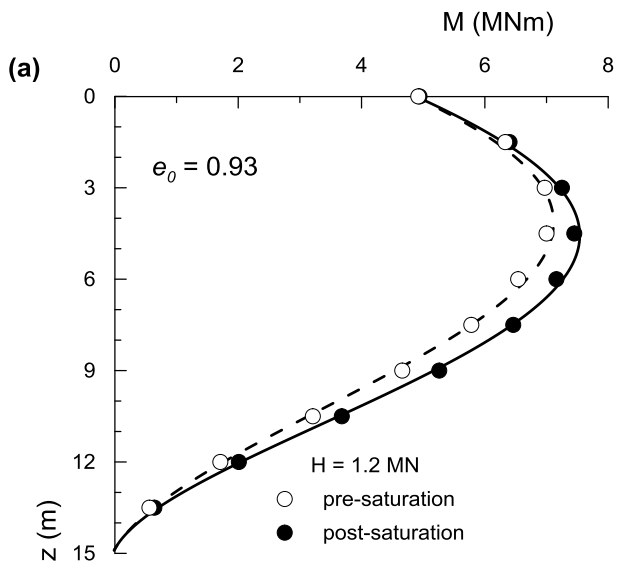


Figure 16: Bending moment profiles before and after saturation: (a) T_06 ($e_0=0.93$), (b) T_08 ($e_0=0.75$).